Paclitaxel induces pyroptosis by inhibiting the volume-sensitive chloride channel leucine-rich repeat-containing 8a in ovarian cancer cells

XIUROU YANG[1*], CHAO LI[1*], XUZHEN LIAO[1], SHIQING LIU[1], XUE LI[2], XIUYING HOU[3], KAI WANG[2], HAIFENG YANG[2], LVFEN GAO[4] and LINYAN ZHU[1]

[1]Department of Pharmacology, School of Medicine, Jinan University, Guangzhou, Guangdong 510632; [2]Department of Pathology, The Second Affiliated Hospital of Guangzhou University of Chinese Medicine (Guangdong Provincial Hospital of Chinese Medicine), Guangzhou, Guangdong 510006; [3]Department of Pathogen Biology, School of Medicine, Jinan University; [4]Department of Obstetrics and Gynecology, The First Affiliated Hospital, Jinan University, Guangzhou, Guangdong 510632, P.R. China

Abstract. Pyroptosis is a newly identified form of cell death, morphologically characterized by excessive cell swelling. In the present study, paclitaxel (PTX) combined with platinum were used as first-line chemotherapy, against ovarian cancer cells by inducing multiple types of cell death. However, it remains unclear whether PTX can induce pyroptosis in ovarian cancer cells. It was recently reported that PTX inhibited chloride channels, an inhibition known to cause cell swelling. In the present study, it was first verified that pyroptosis-like cell death, as well as cleaved-caspase-3 and cleaved-gasdermin E (GSDME) were induced by PTX in A2780 ovarian cancer cells. PTX inhibited the background- and hypotonicity-activated chloride currents, promoted intracellular chloride ion accumulation, those manifestations are similar to those of the classic volume-regulatory anion channel (VRAC) blocker, 4-(2-butyl-6,7-dichloro-2-cyclopentyl-indan-1-on5-yl) oxobutyric acid (DCPIB). Of note, both DCPIB and the downregulation of VRAC constituent protein leucine-rich repeat-containing 8a themselves could not induce persisted cell swelling and pyroptosis-like phenotypes. However, they could enhance the effects of PTX in inducing pyroptosis-like phenotypes, such as marked cell swelling, cell membrane rupture and excessive activation of caspase-3 and GSDME N-terminal fragment, which ultimately caused marked pyroptosis in A2780 cells. These findings revealed a potential mechanism of PTX and offered new insights into the effects of a synergistical combination of PTX and VRACs blockers in ovarian cancer chemotherapy.

Introduction

Pyroptosis, as a lytic programmed cell death, is mediated by the gasdermin family of proteins and is common in inflammatory cells (1). Cell pyroptosis is mainly formed by caspase-1/3/4/5/11 cutting the gasdermin family of proteins to form an N-terminal structure, and is then transferred to the cell membrane for cutting and perforation, in order that cell content can be released (2-4). It is characterized by nuclear aggregation, formation of a large number of 1-2-nm holes on the cell membrane, cell swelling, dissolution and rupture of the plasma membrane, as well as release of inflammatory factors (such as IL-1β and IL-18) to further amplify the inflammatory response (5,6).

As aforementioned, one of the significant morphological features of pyroptosis is excessive cell swelling, which signifies that the capacity of cell volume regulation, particularly regulatory volume decrease (RVD), is impaired. Several studies, including a previous study by the authors, verified that cells could regulate their volume to counteract osmotic swelling, as well as during cell division, growth, migration and cell death by RVD (7-11). Volume-regulated anion channels (VRACs) were activated by hypotonic-stimulus and played pivotal roles in RVD (12). VRAC inhibition could decrease the capacity of RVD, ultimately resulting in cell swelling (8,9,13-15). At present, the involvement of chloride channels in cell pyroptosis is poorly understood. Recently, Ye et al (16) proposed that lipopolysaccharides (LPS) and nigericin, the classic pyroptosis inducers, can decrease the hypotonicity-activated chloride currents and the capability

Correspondence to: Dr Lvfen Gao, Department of Obstetrics and Gynecology, The First Affiliated Hospital, Jinan University, 601 Huangpu Dadao West, Guangzhou, Guangdong 510632, P.R. China
E-mail: freshlucy07@126.com

Professor Linyan Zhu, Department of Pharmacology, School of Medicine, Jinan University, 601 Huangpu Dadao West, Guangzhou, Guangdong 510632, P.R. China
E-mail: tzhuly@jnu.edu.cn

*Contributed equally

of RVD in bone marrow-derived macrophages (BMDMs). In addition, leucine-rich repeat-containing 8a (LRRC8A), the constituent protein of VRACs, was significantly downregulated in pyroptotic BMDMs treated with LPS and nigericin. These results indicated that VRAC/LRRC8A was involved in the pyroptosis of BMDM cells induced by LPS and nigericin.

The mechanisms of pyroptosis in cancer and immune cells appear to be different. Recently, the roles of pyroptosis in cancer and the developments in inducing pyroptosis for cancer therapy have attracted the attention of researchers (17). Paclitaxel (PTX) plus platinum were used as first-line chemotherapy against ovarian cancer (18). To date, PTX has been proven to be closely associated with cell pyroptosis in a number of studies. On the one hand, PTX can induce pyroptosis in nasopharyngeal carcinoma cells through the caspase-1/gasdermin D (GSDMD) pathway (19), and in lung cancer through caspase-3/gasdermin E (GSDME) activation (20). On the other hand, PTX can enhance innate immunity by promoting PYD domains-containing protein 3 (NLRP3) inflammasome activation in macrophages and inducing cell pyroptosis by enhancing the cleavage of GSDMD (21). A previous study by the authors reported that PTX inhibited the background chloride currents, hypotonicity- and cisplatin-activated chloride currents in A2780 ovarian cancer cells (22). It is well known that blocking chloride channels inhibited the RVD, ultimately causing cell swelling (23,24). Therefore, in the present study, whether PTX could induce cell swelling and finally lead to ovarian cancer cell pyroptosis by inhibiting chloride channels was investigated.

Materials and methods

Cell culture. A2780 (cat. no. CC0803; https://www.culturecollections.org.uk/collections/ecacc.aspx) and SKOV3 (cat. no. CC0801; https://www.ATCC.org/) human ovarian cancer cell lines were purchased from Guangzhou Cellcook Biotech Co., Ltd. A2780 and SKOV3 cells were cultured in DMEM (Gibco; Thermo Fisher Scientific, Inc.) supplemented with 10% FBS (Biological Industries) and 100 μg/ml penicillin and 100 μg/ml streptomycin (Gibco; Thermo Fisher Scientific, Inc.). Cells were cultured at 37˚C in a humidified atmosphere containing 5% CO_2. A2780 was subcultured every 2 days, and SKOV3 was subcultured every 3 days. In subsequent cell experiments, DMSO was used as the solvent control by default for PTX.

Cell viability assay and half maximal inhibitory concentration (IC_{50}) measurement. The effect of PTX on A2780 and SKOV3 cell viability was evaluated by MTT assay. Cells were seeded in 96-well plates with a density of 7,000-8,500 cells/well and cultured overnight at 37˚C with 5% CO_2. The cells were exposed to PTX (0, 0.5, 1, 2, 4, 8, 16, 32, 64, 128 and 256 nM) in culture medium for 24 and 48 h respectively. Next, 20 μl of 5 mg/μl MTT was added to each well and incubated for 4 h. After the supernatant was removed, 150 μl dimethyl sulfoxide was added to each well. Finally, the plates were shaken for 10 min to fully dissolve the formation crystals. All experiments were carried out in the dark. Subsequently, an infinite M200PRO microplate reader (Bio-Rad Laboratories, Inc.) was used to measure the optical density (OD) value at

an absorbance of 490 nm. The IC_{50} values for each group of cells were determined using the following formula: Inhibition (%)=($OD_{control}$-OD_{test})/$OD_{control}$ x100%.

Cell apoptosis assay by flow cytometry and Annexin V-FITC-A double staining. For cell apoptosis analysis, A2780 and SKOV3 cells were seeded in 6-well plates at a density of 15,000 cells/well overnight. A2780 was treated with 10 nM PTX for 24 h at 37˚C and SKOV3 was treated with 10 and 250 nM PTX for 48 h at 37˚C. Following collection, the cells were washed with ice-cold PBS twice, and fixed with 70% ethanol at -20˚C for >4 h. Next, the collected cells were stained with 400 μl propidium iodide (PI) at room temperature for 30 min. Finally, cell apoptosis distribution was examined by flow cytometry (BD FACSCanto 8.0; Beckman Coulter, Inc.). Data were analyzed using the Modfit program (version 8.0; BD Biosciences).

Cell volume assay by flow cytometry. As for volume analysis, cells were seeded in six-well plates with a density of 15,000 cells/well overnight. A2780 was treated with 10 nM PTX for 0-24 h at 37˚C and SKOV3 was treated with 250 nM PTX for 0-48 h at 37˚C. Following collection, the cells were washed with ice-cold PBS twice, and fixed with 70% ethanol at -20˚C for >4 h. Following fixation, the fixation solution was removed and the cells were collected again and resuspended in PBS. The forward scattered light (FSC) was proportional to the cell volume. Finally, FSC was examined by flow cytometry (BD FACSCanto 8.0; Beckman Coulter, Inc.). All data were analyzed using the Modfit program (version 8.0; BD Biosciences).

Lactate dehydrogenase (LDH) release assay and PI staining. LDH release in cells was assessed using an LDH Cytotoxicity Assay Kit (cat. no. C0017; Beyotime Institute of Biotechnology) with a full-wavelength enzyme reader (Thermo Fisher Scientific, Inc.), according to the manufacturer's instructions. In brief, 120 μl of the supernatant culture medium of A2780 and SKOV3 cells treated with PTX were collected in a 96-well plate, and the response mixture was added and incubated in the dark for 30 min at room temperature. The absorbance value at 490 nm was then measured, referenced by 600 nm.

The A2780 and SKOV3 cells were cultured for 15 min with 2.5 μg/ml PI at 20˚C (cat. no. 556463; BD Biosciences). At the end of the incubation, cells were slowly washed with PBS twice. The cells were then exposed to 1 μg/ml Hoechst 33342 (cat. no. C1022; Beyotime Institute of Biotechnology) for 5 min at 20˚C, and observed under a fluorescence microscope.

Scanning electron microscopy (SEM). Cell morphology was monitored by SEM: Following fixing in 2.5% glutaraldehyde overnight at 20˚C, cells were dehydrated through a graded series of ethanol (30, 50, 70, 95 and 100%) and treated for 5 min at each concentration. The alcohol in the sample was gradually replaced with isoamyl acetate, then were critical-point dried. Dried specimens were chilled at -80˚C and transferred to a freezing dryer overnight. Each sample was coated with gold-palladium and imaged by SEM (S-3400 N; Hitachi Science Systems Ltd.).

Reverse transcription-quantitative PCR (RT-qPCR). Total RNA from A2780 cells was obtained using Total RNA Extraction Kit (cat. no. RIJ26-01; Magen Biotechnology Co., Ltd.) and reversed-transcribed to cDNA with a Prime ScriptRT reagent (cat. no. RR037A; Takara Bio, Inc.), according to the manufacturer's instructions. The amplification of cDNA was performed using TB Green Premix Ex Taq (cat. no. RR820A; Takara Bio, Inc). The parameters of a real-time system (CFX Connect; Bio-Rad Laboratories, Inc.) were set at 95˚C for 30 sec, followed by 40 cycles of 5 sec at 95˚C and 30 sec at 60˚C. The primers used are listed in Table I. Quantification of gene expression was performed by quantification curve. The expression levels of the target genes were quantitated using the $2^{-\Delta\Delta Cq}$ method and GAPDH was used as the internal control to normalize the qPCR data (25).

Western blotting for protein expression. Cells were washed with ice-cold PBS, and lysed with cell lysis buffer for western blotting and IP (cat. no. P0013; Beyotime Institute of Biotechnology) containing 1% PMSF. Protein lysates were quantified using the BCA Protein Assay Kit (cat. no. KGP903; Nanjing KeyGEN Biotech Co., Ltd.). Equal amounts of protein (20 μg) were separated using 10% SDS-PAGE and transferred onto PVDF membranes (cat. no. PR 05505; MilliporeSigma). Following blocking with 5% non-fat milk in Tris-buffered saline with Tween-20 (0.05%) at room temperature for 2 h, the membranes were incubated with rabbit anti-LRRC8A primary antibody (cat. no. 24979S; dilution, 1:800; Cell Signaling Technology, Inc.), rabbit anti-ClC-2 primary antibody (cat. no. ab192526; dilution, 1:800; Abcam), rabbit anti-ClC-3 primary antibody (cat. no. ab28736; dilution, 1:1,000; Abcam), rabbit anti-anoctamin-1 (ANO1) primary antibody (cat. no. ab64085; dilution, 1:800; Abcam), rabbit anti-caspase-3 primary antibody (cat. no. ab49822; dilution, 1:600; Abcam), rabbit anti-GSDME primary antibody (cat. no. ab215191; dilution, 1:800; Abcam) and rabbit anti-GAPDH antibody (cat. no. RIP008; dilution, 1:1,000; Beijing Dingguo Changsheng Biotechnology Co. Ltd.) overnight at 4˚C. Membranes were then incubated for 2 h at room temperature with HRP-linked goat anti-rabbit secondary antibody (dilution, 1:10,000; cat. no. IH-0011; Beijing Dingguo Changsheng Biotechnology Co. Ltd.). Proteins were visualized using Ultra High Sensitivity ECL Kit (GlpBio Technology, Inc.). Images were acquired and quantified using the gel imaging system (Alliance 4.7; Bio-Rad Laboratories, Inc.).

Whole-cell current recording. Whole-cell chloride currents were measured using a patch clamp amplifier system (EPC-10; HEKA GmbH Technology & Trade). The pipette solution contained 70 mM N-methyl-d-glucamine, 1.2 mM MgCl$_2$, 10 mM N-2-hydroxyethylpiperazine-N'-2-ethanesulfonic acid (HEPES), 1 mM ethylene glycol tetraacetic acid, 140 mM D-mannitol and 2 mM adenosine triphosphate, with a pH of 7.25 and osmolality of 300 mOsm/kg·H$_2$O. The isotonic bath solution contained 70 mM NaCl, 0.5 mM MgCl$_2$, 2 mM CaCl$_2$, 10 mM HEPES and 140 mM D-mannitol, pH 7.4, osmolality 300 mOsm/kg·H$_2$O. The 47% hypotonic bath solution was similar to the isotonic bath solution, except for D-mannitol,

Table I. Sequences of the primers for reverse transcription-quantitative PCR.

Gene name	Primer sequence (5'→3')
GSDMD	F: GTGTGTCAACCTGTCTATCAAGG
	R: CATGGCATCGTAGAAGTGGAAG
GSDME	F: ACATGCAGGTCGAGGAGAAGT
	R: TCAATGACACCGTAGGCAATG
Caspase-1	F: ATGTCTGTGGGCAGGAAGTG
	R: CCCTGTTTCTTCAGTGTGGGA
Caspase-3	F: CATGGAAGCGAATCAATGGACT
	R: CTGTACCAGACCGAGATGTCA
Caspase-4	F: CAAGAGAAGCAACGTATGGCA
	R: AGGCAGATGGTCAAACTCTGTA
Caspase-5	F: TTCAACACCACATAACGTGTCC
	R: GTCAAGGTTGCTCGTTCTATGG
GAPDH	F: GGTGGTCTCCTCTGACTTCAACA
	R: GTTGCTGTAGCCAAATTCGTTGT

F, forward; R, reverse; GSDM, gasdermin; CASP, caspase.

and its osmolality was 160 mOsm/kg·H$_2$O. All chemicals were the highest grade available and purchased from Sigma-Aldrich (Merck KGaA).

A2780 cells (20,000 cells/ml) plated on coverslips were washed with the isotonic bath solution. The whole-cell current was recorded with a resistance of 4-5 MΩ under the aforementioned patch-clamp amplifier (EPC-10) using patch-clamp pipettes, which were made from glass microtubules on a two-stage vertical pipette puller (PC-10; Sutter Instrument Company). Cell membrane potential was held at the Cl⁻ equilibrium potential (0 mV) and repeatedly stepped to 0, ±40 and ±80 mV for 200 msec pulses in 4 sec throughout the experiments. A computer recorded the whole-cell currents using a laboratory interface (MICRO 1401-4; Cambridge Electronic Design, Ltd.) at a sampling rate of 3 kHz. All experiments were processed at room temperature (20-24˚C). The inhibition rate of PTX of the background Cl⁻ current was calculated using the following equation: Inhibition (%)=(CIso-CIso + PTX)/CIso x100%. The inhibition rate of PTX of the hypotonicity-activated Cl⁻ current was calculated using the following equation: Inhibition (%)=(Chypo-Chypo + PTX)/Chypo x100%, where CIso is the background current under isotonic condition, Chypo is the peak value of hypo-activated currents, and CIso + PTX and Chypo + PTX are the currents recorded after adding PTX in isotonic or hypotonic solution.

Measurement of intracellular chloride ion concentration ([Cl⁻]i). Ovarian cancer cells A2780 were washed with Krebs-HEPES buffer (20 mM HEPES, 128 mM NaCl, 2.5 mM KCl, 2.7 mM CaCl$_2$, 1 mM MgCl$_2$, 16 mM glucose, pH 7.4) and exposed to 10 mM N-(ethoxycarbonylmethyl)-6-methoxyquinolinium bromide (MQAE; Beyotime Institute of Biotechnology), a novel fluorescent probe for Cl⁻ whose fluorescence intensity quenches when it binds to Cl⁻, for 60 min at 37˚C and washed again with

Krebs-HEPES buffer. 4-(2-butyl-6,7-dichloro-2-cyclopentyl-indan-1-on5-yl) oxobutyric acid (DCPIB; MedChemExpress) was configured as a 5 mM high-concentration storage solution with DMSO. This was then further diluted with PBS to a concentration of 1 μM. Fluorescence emission was used to detect the fluorescence intensity of MQAE and quantify the concentration of Cl⁻, including inverted fluorescence photography and real-time fluorescence detection. Real-time fluorescence detection used fast laser scanning confocal microscopy (cat. no. SP8; Leica Microsystems, Inc.) to detect cellular fluorescence. The instrument first recorded the fluorescence intensity of the cells without drug stimulation for ~5 min, added the Krebs-Hepes buffer containing purple stripes according to the experimental needs and recorded the changes of MQAE fluorescence intensity following drug stimulation.

Small interfering RNA (siRNA) transfection. A2780 ovarian cancer cells were transfected (37˚C for 8 h) using GP-transfect-mate (4 μl in 500 μl serum-free medium; Shanghai GenePharma Co., Ltd.) transfection reagents with siRNA (0.16 μM) targeting human LRRC8A (Shanghai GenePharma Co., Ltd.). The time interval between transfection and subsequent experiments was 48 h. The siRNA target sequences used are presented in Table II.

Statistical analysis. Data are presented as the mean ± SEM. Comparative studies of means were performed using one-way analysis of variance (ANOVA) followed by a post hoc test (projected least significant difference Fisher). Differences between two groups were assessed using an unpaired Student's t-test, and between paired variables were assessed using a paired Student's t-test. Dunnett's t-test was used to compare the differences between the control group and multiple experimental groups. $P<0.05$ was considered to indicate a statistically significant difference.

Results

PTX induces pyroptosis-like cell death in A2780 ovarian cancer cells. The cell viability of A2780 and SKOV3 ovarian cancer cell lines was inhibited to various degrees following treatment with PTX at concentrations of 0.5-256 nM for 24-48 h. As shown in Fig. 1A and B, the IC_{50} in A2780 cells following treatment with PTX for 24 h was 9.67±1.46 nM, while little inhibition can be observed in SKOV3 cells. Following treatment with PTX for 48 h, the IC_{50} in A2780 cells and SKOV3 cells were 3.23±0.33 and 221.9±31.72 nM ($P<0.001$ vs. A2780, n=4), respectively. Flow cytometry revealed a higher level of necrosis (Annexin V⁺/PI⁺ cells) as compared with that of apoptosis (Annexin V⁺/PI⁻ cells) in A2780 cells (Fig. 1C and D) following 10 nM PTX treatment for 24 h. However, apoptosis was dominantly exhibited in SKOV3 cells treated with 250 nM PTX for 48 h (Fig. 1C and E).

Similarly, Hoechst 33342/PI staining also demonstrated that the ratio of necrosis (PI⁺ cells) was markedly elevated in A2780 cells following treatment with PTX (Fig. 1F-G; $P<0.001$; n=3). The effect of PTX on plasma membrane damage was evaluated by measuring LDH release in the culture supernatant. LDH release was significantly increased

Table II. siRNA target sequences.

siRNA name	Sequence (5'→3')
LRRC8A siRNA1	F: GCAGCAACUUCUGGUUCAATT
	R: UUGAACCAGAAGUUGCUGCTT
LRRC8A siRNA2	F: CCUCAAGAAGUACUCGUUUTT
	R: AAACGAGUACUUCUUGAGGTT
LRRC8A siRNA3	F: GCCUUAAGCUGUGGUACAATT
	R: UUGUACCACAGCUUAAGGCTT
Negative control	F: UUCUCCGAACGUGUCACGUTT
siRNA	R: ACGUGACACGUUCGGAGAAT

F, forward; R, reverse; siRNA, small interfering RNA; LRRC8A, leucine-rich repeat-containing protein 8A.

in A2780 cells following treatment with 10 nM PTX compared with the control group (Fig. 1H; $P<0.001$; n=3), while it was increased in SKOV3 cells at a PTX concentration of 250 nM. These results indicated that PTX induced cell death by causing plasma membrane damage in ovarian cancer cells.

PTX-induced cell swelling and cleavage of caspase-3/GSDME in A2780 cells. Membrane rupture and cell swelling induced by cleaved gasdermin family members are the main morphological characteristics of pyroptosis (26). In the present study, the volume of A2780 cells was gradually increased following treatment with PTX 10 nM for 1.5-24 h (Fig. 2A), suggesting cell swelling, while no obvious changes were observed in SKOV3 cells (Fig. 2B). The volume only increased after 12 h of 250 nM PTX treatment in SKOV3 cells (Fig. 2C). Therefore, the next experiments focused on A2780 cells.

The morphological changes of A2780 cells were then examined by SEM. As revealed in Fig. 2D, the membrane surface of normal cells was intact and relatively smooth. Following treatment with PTX, the cells were swollen with pores and evident large bubbles extending from the plasma membrane, suggesting the occurrence of a distinct morphological change characteristic of pyroptosis (5).

GSDMD and GSDME are common executive proteins in pyroptosis, and the GSDME protein is highly expressed in ovarian tissue (27,28). However, it is unclear which member of the gasdermin family is involved in the induction of pyroptosis by PTX. In the present study, the genes associated with pyroptosis were screened using RT-qPCR. The results showed that GSDME, caspase-3 and caspase-4 genes were mainly expressed in A2780 cells, and the expression of both caspase-3 and GSDME were increased while that of caspase-4 was significantly decreased following treatment with PTX (Fig. 2E and F). At the protein level, PTX also induced the cleavage of caspase-3 and GSDME, creating cleaved caspase-3 (cl-caspase-3) and GSDME N-terminal fragment (GSDME-N), respectively, in A2780 cells (Fig. 2G and H). These results indicated that PTX induced pyroptosis through the caspase-3/GSDME pathway in A2780 cells.

PTX inhibits chloride currents and increases [Cl⁻]i in A2780 cells. The above data showed that PTX can cause cell swelling.
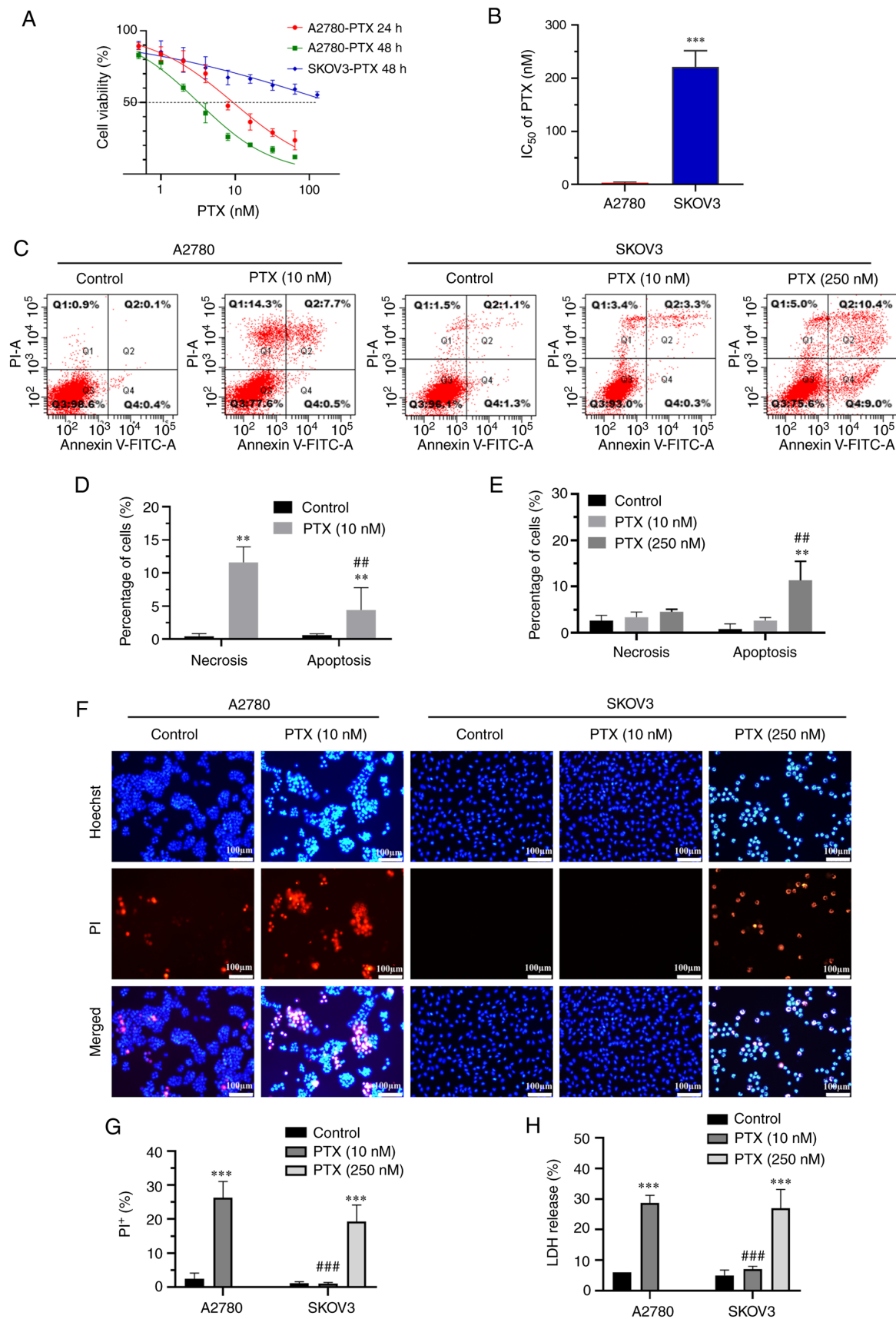
Figure 1. PTX induces pyroptosis-like cell death in A2780 ovarian cancer cells. (A and B) Different effects of PTX on the viability of A2780 ovarian cancer cells and SKOV3 cells treated with PTX for 24 and 48 h, respectively (n=4 for both; ***P<0.001 vs. A2780 cells). (C-E) Representative analysis of flow cytometry and percentage of apoptosis (stained with Annexin V+/PI-) or necrosis (stained with Annexin V+/PI+) induced by 10 nM PTX in A2780 cells at 24 h, and 10 and 250 nM PTX in SKOV3 cells at 48 h (n=4; **P<0.01 vs. Control; and ##P<0.01 vs. necrosis). (F and G) Photomicrographs of double-fluorescent staining with Hoechst 33342 (blue) and PI (red) was acquired with or without PTX for 48 h (n=3; ***P<0.001 vs. Control; and ###P<0.001 vs. A2780 cells treated with 10 nM PTX). (H) Effects of PTX on LDH release in the supernatant was determined by LDH release assay (n=3; ***P<0.001 vs. Control; and ###P<0.001 vs. A2780 cells treated with 10 nM PTX). PTX, paclitaxel; PI, propidium iodide; LDH lactate dehydrogenase.
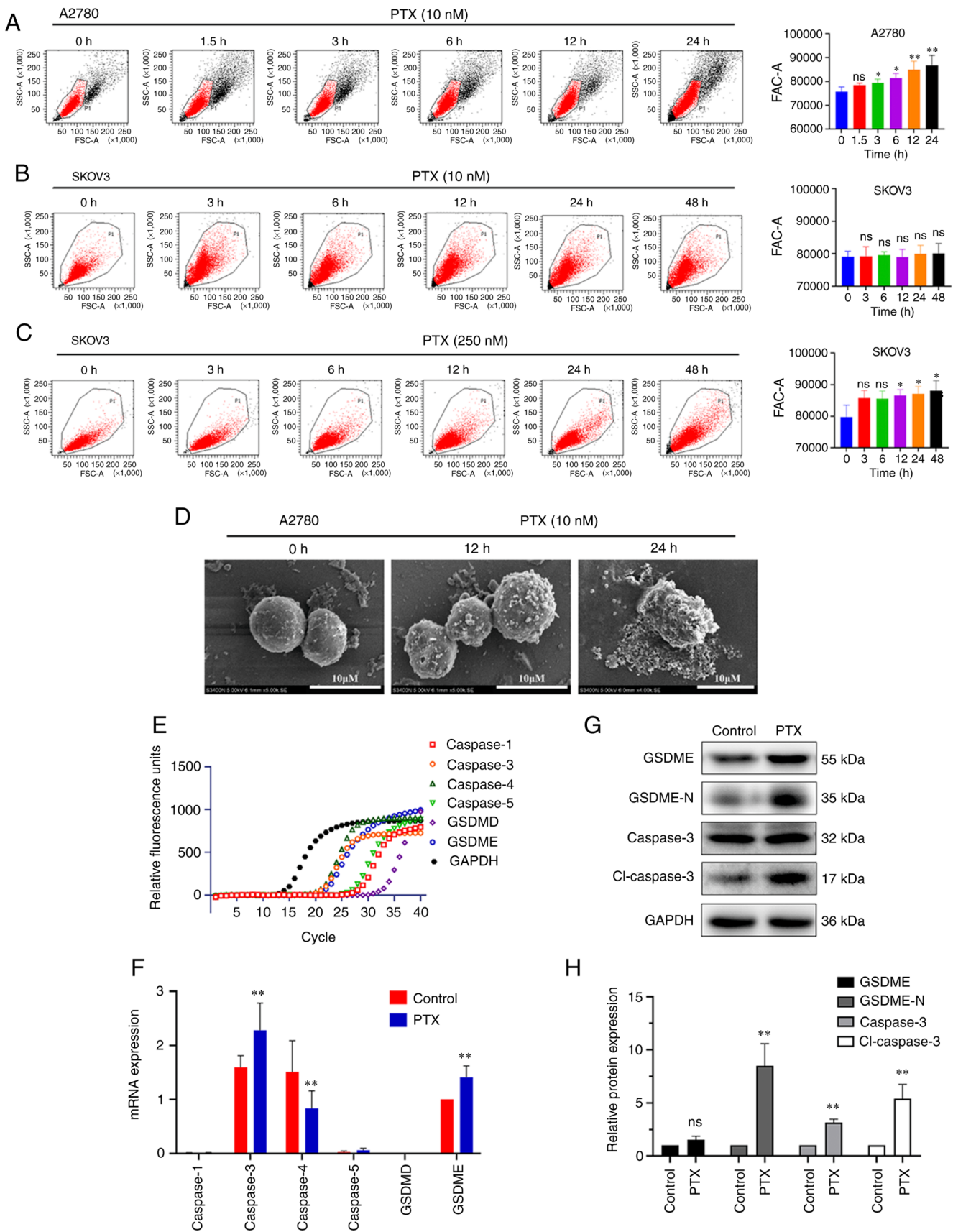
Figure 2. PTX induces pyroptosis in ovarian cancer cells through the caspase-3/GSDME pathway. (A-C) Flow cytometry was used to detect the effect of PTX on the volume of A2780 and SKOV3 ovarian cancer cells. The A2780 ovarian cancer cell line was treated with 10 nM PTX and the SKOV3 ovarian cancer cell line with 10 or 250 nM PTX for different time points (n=4; $^*P<0.05$ and $^{**}P<0.01$; ns>0.05). (D) Scanning electron micrographs of A2780 cells treated with 10 nM PTX for 12 and 24 h (scale bar, 10 μm). (E and F) Relative fluorescence units of caspases-1/3/4/5, GSDMD, GSDME and GAPDH mRNA in A2780 cells in the control and PTX treatment groups, as detected by reverse transcription-quantitative PCR (n=3; $^{**}P<0.01$ vs. Control). (G and H) Protein expression levels of full-length GSDME, GSDME-N, caspase-3 and cl-caspase-3 were assessed using western blotting (n=3; $^{**}P<0.01$ vs. Control). PTX, paclitaxel; GSDMD, gasdermin D; GSDME, gasdermin E; GSDME N-terminal fragment; ns, not significant; cl-caspase-3, cleaved-caspase-3.

A previous study by the authors revealed that PTX inhibited background- and hypotonicity-activated chloride currents in A2780 cells (22). In addition, it has previously been revealed that the inhibition of the chloride channel caused an increase in the cell volume (23,29). Herein, it was also confirmed that the inhibition of background- and hypotonicity-activated chloride currents by PTX was similar to the effect of classic VRAC inhibitor, DCPIB (Fig. 3A and B). It is known that the inhibition of chloride currents leads to a decrease in Cl⁻ efflux. In the present study, the MQAE fluorescence intensity was significantly decreased following treatment with DCPIB and PTX, which indicated that the [Cl⁻]i increased (Fig. 3C and D). Real-time fluorescence assay also showed that the [Cl⁻]i increased following treatment with PTX and DCPIB (Fig. 3E and F). The statistical analysis results are shown in Fig. 3G. These results suggested that PTX can inhibit the volume-sensitive chloride channels in the same way as DCPIB, and cause an increase in the [Cl⁻]i.

The component of volume-activated chloride channels, LRRC8A, is influenced by PTX in A2780 cells. There are several molecular categories of volume-activated chloride channel proteins (7). In the present study, RT-qPCR was used to detect the mRNA expression of the chloride channels of ClC-2/ClC-3/ANO1/LRRC8A in A2780 cells. As revealed in Fig. 4A and B, volume-sensitive or volume-related chloride channel genes expressed in A2780 cells mainly included ClC-2, ClC-3 and LRRC8A. Only the LRRC8A mRNA expression was increased, while that of the other genes exhibited no significant changes following treatment with PTX. Similar to the mRNA expression results, the protein expression of LRRC8A was significantly increased following PTX treatment, while the expression of the other proteins did not exhibit any significant changes (Fig. 4C-G). It was therefore inferred that LRRC8A may be involved in PTX-induced pyroptosis in A2780 cells.

The VRAC inhibitor, DCPIB, or the downregulation of LRRC8A protein enhance the efficacy of PTX-induced pyroptosis in A2780 cells. VRAC plays a major role in cell volume regulation, and its main component is LRRC8A (30). To further investigate the role of VRAC in cell pyroptosis, PTX combined with VRAC inhibitor, DCPIB, or LRRC8A siRNA (Fig. S1; the si-L-3 sequence was selected by default for the subsequent downregulation of LRRC8A) was used in the experiment. In the experimental group, the concentration of PTX-treated cells was 10 nM and the treatment time was 24 h. As shown in Fig. 5A and B, DCPIB or si-LRRC8A alone had no effect on LDH release. However, both markedly enhanced the PTX-induced LDH release. The effect of DCPIB and si-LRRC8A on cell volume was investigated, and the cells in the combination group were found to be larger, while DCPIB or siRNA alone had little effect on cell volume (Fig. 5C-F). Next, the morphological changes of the cells were examined using SEM. Consistently, it was found that A2780 cells treated with DCPIB or si-LRRC8A combined with PTX for 24 h exhibited more severe cell membrane damage and could not maintain a normal morphology compared with cells treated with PTX alone (Fig. 5G). However, the treatment of cells with DCPIB or si-LRRC8A alone had little effect on cell morphology.

According to these results, the inhibition of VRAC function or the decrease in LRRC8A protein expression could enhance the degree of PTX-induced pyroptosis.

DCPIB or si-LRRC8A increases the expression of pyroptosis-related proteins in A2780 cells. Given that the inhibition of VRAC combined with PTX can increase pyroptosis in A2780 cells, the changes in pyroptosis-related proteins, including caspase-3, cl-caspase-3, GSDME and GSDME-N were further investigated. The levels of pyroptosis proteins, such as cl-caspase-3 and GSDME-N, were significantly increased by DCPIB/si-LRRC8A and PTX combination therapy, as compared with those following treatment with PTX alone (Fig. 6A-D and F and G). However, there was no significant change in pyroptosis-related protein following treatment with DCPIB or si-LRRC8A alone. In addition, cells treated with si-LRRC8 combined with PTX showed an increase in LRRC8 protein compared with si-LRRC8 alone (Fig. 6E). These results indicated that the inhibition of VRAC or decrease in LRRC8A expression promoted PTX-induced pyroptosis in A2780 cells.

Discussion

PTX was first approved for the treatment of ovarian cancer (31), with its application expanding into various other types of cancer some years later (32-34). To date, it is well known that PTX can induce multiple types of cell death, including mitotic catastrophe, apoptosis, senescence, autophagy and pyroptosis (35). In the present study, it was first observed that A2780 ovarian cancer cells exhibited features of pyroptosis, such as cell swelling, LDH release, deep PI staining and membrane perforation. As shown by SEM, A2780 cells exhibited evident swelling, and characteristic large bubbles appeared from the plasma membrane following PTX treatment. These data demonstrated that pyroptosis may be one of the underlying mechanisms of PTX for the treatment of ovarian cancer.

The gasdermin family of proteins plays a key role in cell pyroptosis. The family comprises six paralogous proteins in humans: GSDMA/B/C/D/E and PJVK (36). GSDMD and GSDME are best known for their functions in pore formation and pyroptosis (17). GSDMD activates cutting via caspases-1/4/5/11 (36), while GSDME activates cutting via caspase-3 (37). PTX has been shown to induce pyroptosis in both caspase-1/GSDMD and caspase-3/GSDME pathways in different types of cancer (19-21). Among ovarian tissues, the gasdermin family proteins mainly express GSDME (27,28). Previous studies have shown that chemotherapy drug-activated caspase-3 can induce secondary necrosis/pyroptosis in both cancer and normal cells that express high levels of GSDME (37-39). In the present study, GSDME was mainly expressed in A2780 cells, while GSDMD expression was very low. The upstream proteins of pyroptosis with the highest expression were caspases-3/4. Caspase-3 and GSDME mRNA expression was increased while caspase-4 mRNA expression was significantly decreased following treatment with PTX. Further western blotting also confirmed that the protein expression of caspase-3 and GSDME-N fragment, which was cleaved by caspase-3, were significantly increased in A2780 cells following treatment with PTX. Therefore, it was inferred
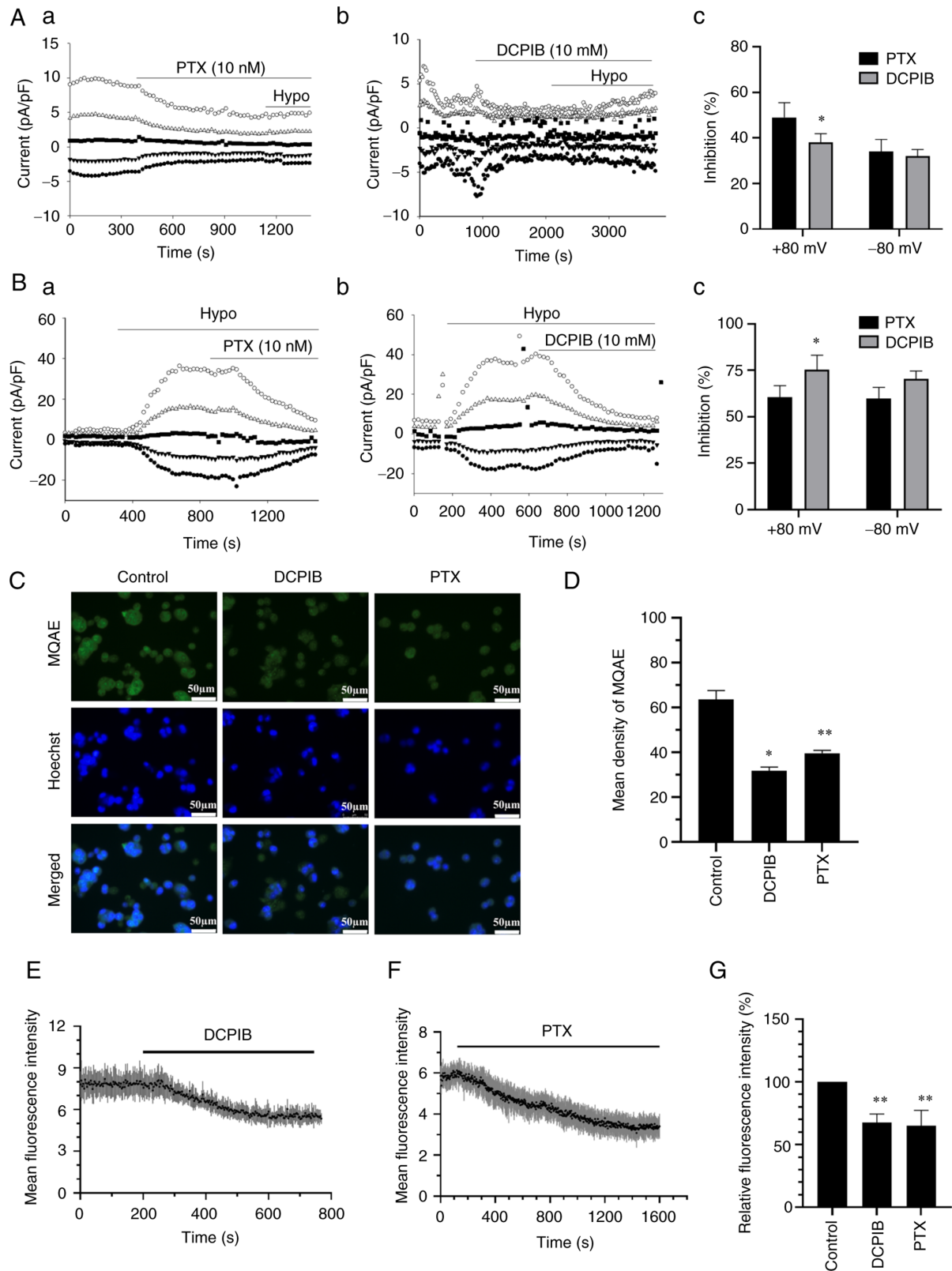
Figure 3. PTX inhibits volume-sensitive chloride channel current and increases intracellular chloride ion accumulation. (A and B) Whole cell recording was used to investigate the function of the chloride channel. The voltage was held at 0 mV and then stepped repeatedly to 0, ±40 and ±80 mV with an interval of 4 sec between steps. The hollow black dots are the chlorine current at +80 and +40 mV voltages, and the solid black dots are the chlorine current at -80 and -40 mV voltages. (Aa-b) The typical time-course of background chloride currents was recorded and influenced by (Aa) PTX or (Ab) DCPIB in A2780 cells. (Ac) The inhibition of background currents by PTX and DCPIB was calculated in A2780 cells (n=4; *P<0.05 vs. the PTX group at +80 mV). (Ba-b) The typical time-course of 47% hypotonicity-activated chloride currents was recorded in A2780 cells inhibited by (Ba) PTX or (Bb) DCPIB. (Bc) The inhibition of 47% hypotonicity-activated chloride currents by PTX and DCPIB was calculated in A2780 cells (n=4; *P<0.05 vs. the PTX group at +80 mV). (C and D) Micrographs of Hoechst 33342 (blue) and MQAE (green) double fluorescence staining were captured using an inverted fluorescence microscope under control conditions, in A2780 cells treated with PTX or DCPIB for 6 h (n=3; *P<0.05 and **P<0.01 vs. Control). (E and F) The fluorescence intensity of MQAE was assessed using a real-time fluorescence assay in A2780 cells treated with PTX and DCPIB. (G) Statistical results of relative fluorescence intensity (n=3; **P<0.01 vs. Control). PTX, paclitaxel; DCPIB, 4-(2-butyl-6,7-dichloro-2-cyclopentyl-indan-1-on5-yl) oxobutyric acid; MQAE, N-(ethoxycarbonylmethyl)-6-methoxyquinolinium bromide.
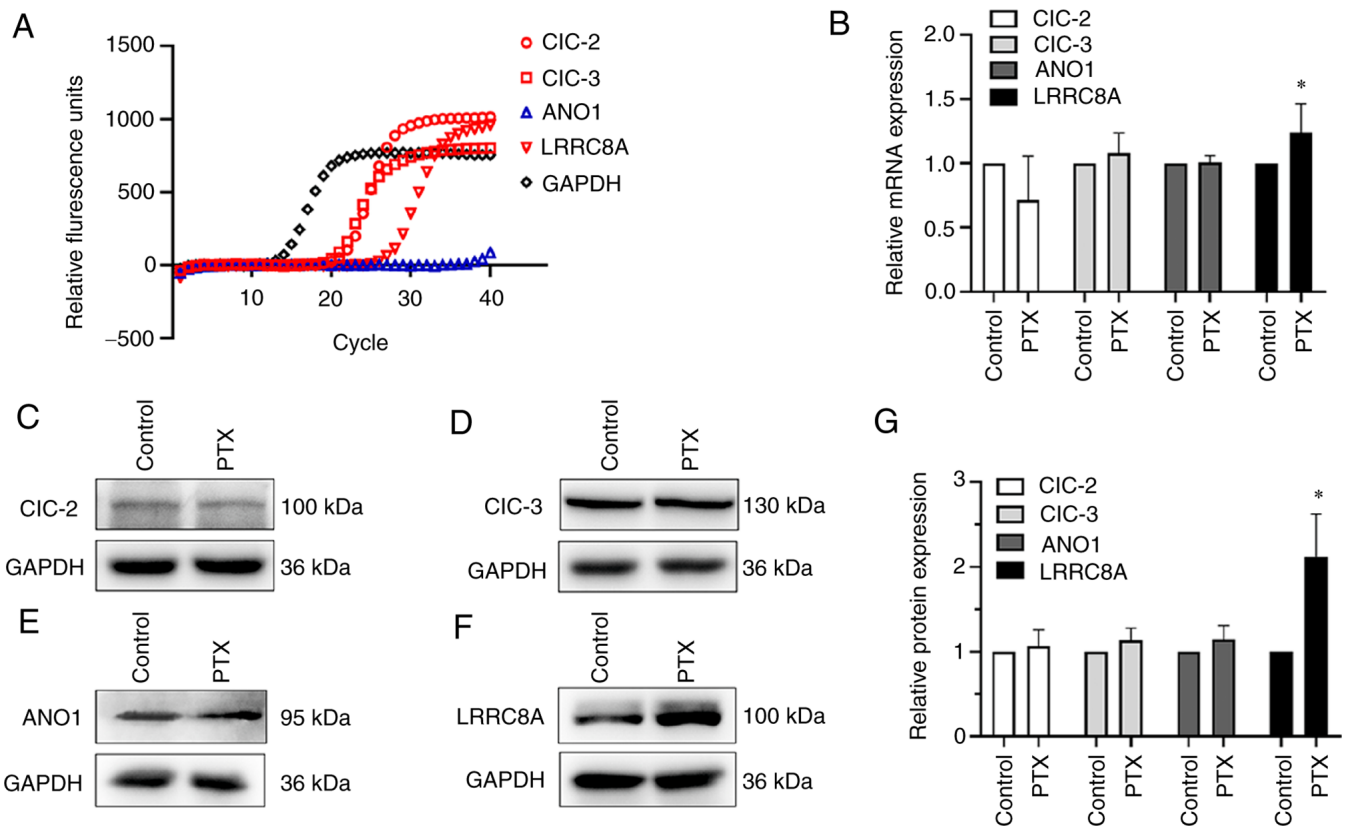
Figure 4. LRRC8A is involved in PTX-induced pyroptosis in A2780 cells. A2780 ovarian cancer cells were treated with 10 nM PTX for 24 h. There were two treatement groups: A control group without PTX (Control) and a PTX-treated group (PTX). (A and B) The relative fluorescence units of ClC-2, ClC-3, ANO1, LRRC8A and GAPDH mRNA in A2780 cells were detected using reverse transcription-quantitative PCR. (n=3; *$P<0.05$ vs. Control). (C-G) The protein expression levels of ClC-2, ClC-3, ANO1 and LRRC8A were assessed using western blotting (n=3; *$P<0.05$ vs. Control). LRRC8A, leucine-rich repeat-containing 8a; PTX, paclitaxel; ClC, chloride channel; ANO1, anoctamin-1.

that PTX induced pyroptosis mainly by activating caspase-3 to cleave GSDME in A2780 ovarian cancer cells.

Following the activation of caspase proteins, gasdermin family proteins have been revealed to cleave to separate their N-terminal pore-forming domain from the C-terminal repressor domain, and finally the N-terminal is inserted into cell membranes and forms large oligomeric pores, disrupting ion homeostasis and subsequently inducing osmotic swelling (27,36). Several studies, including the present one, have demonstrated that the blockage of chloride channels led to cell swelling in both isotonic and hypotonic conditions (8,23,29,40). It was also demonstrated that PTX could inhibit the background-, hypotonicity- and cisplatin-induced chloride currents in A2780 ovarian cancer cells (22). It was also confirmed herein that PTX inhibited the basic/background- and hypotonic-induced chloride currents of A2780 cells, and increased the [Cl⁻]i, which may decrease the passive water efflux and cause osmotic swelling. The above phenomena were also induced by DCPIB, a classic blocker of VRACs. It could therefore be deduced that the inhibition of chloride channels by PTX may contribute to the underlying mechanism of cell swelling in the formation of pyroptosis. However, it has also been reported that Cl⁻ outflow can initiate and activate NLRP3 inflammasomes by promoting the polymerization of ASC, and then induce caspase-1/GSDMD pathway-mediated pyroptosis (41,42). Therefore, the flow direction of chloride

ions on both sides of the cell membrane is likely to be different during pyroptosis and to depend on different cell types and pyroptosis inducers.

The candidate proteins for VRACs have been debated for years. LRRC8A was identified as an essential component of the VRACs in 2014 (30). In the present study, the expression of LRRC8A, ClC-2, ClC-3 and ANO1, which have been proposed to be associated with VRACs, were measured. Only LRRC8A was overexpressed, which was inconsistent with the findings of a previous study by Ye et al (16), which reported that LRRC8A expression was reduced during pyroptosis in BMDM cells induced by LPS and nigericin. Even in the present study, the increased LRRC8A protein expression was inconsistent with the PTX-induced inhibition of chloride currents. DCPIB is a known specific and potent inhibitor of VRAC (43). Unlike the inhibition by si-RNA, the inhibition by DCPIB is completely reversible (44). In recent years DCPIB has been increasingly used for probing the physiologic and pathologic roles of VRAC. Ye et al (16) reported that VRAC inhibitors, such as DCPIB and tamoxifen, and LRRC8A downregulation by siRNA interference can induce pyroptosis-like phenotypes similar to those by LPS and nigericin in BMDM cells. However, the present findings showed that DCPIB and LRRC8A siRNA alone did not cause pyroptosis in A2780 ovarian cancer cells, but could enhance the activities of PTX in inducing pyroptosis. A reason why VRACs exhibit these differences during the
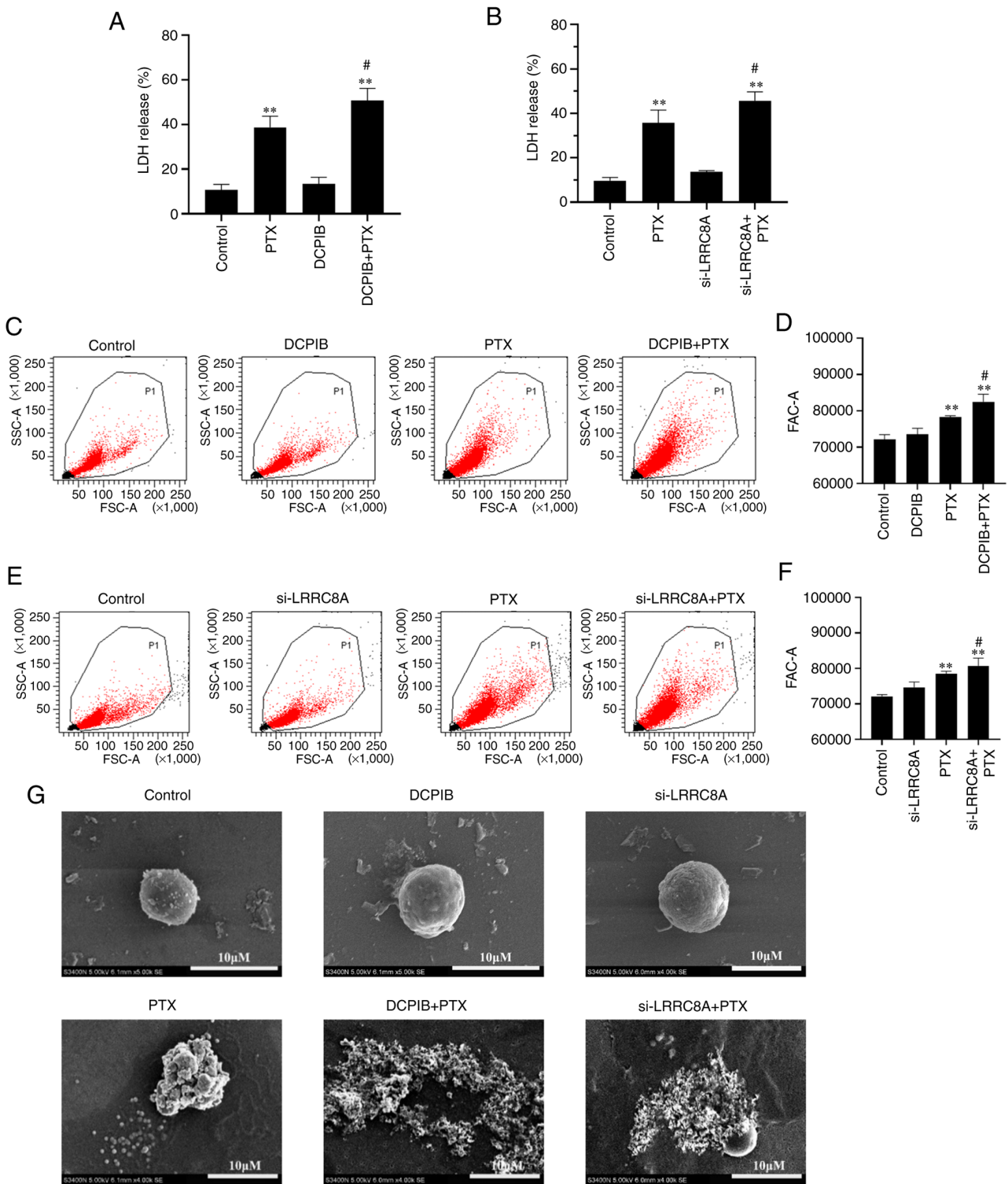
Figure 5. DCPIB and si-LRRC8A enhance PTX-induced pyroptosis. The effect of (A) DCPIB or (B) si-LRRC8A combined with PTX treatment on LDH release was determined using an LDH release assay (n=3; **P<0.01 vs. Control; and #P<0.05 vs. the PTX group). Flow cytometry was used to determine the cell volume of A2780 cells. (C and D) The combination of PTX and DCPIB or (E and F) si-LRRC8A led to significant cell swelling compared with PTX alone in A2780 cells (n=3; **P<0.01 vs. Control; and #P<0.05 vs. the PTX group). (G) Cell morphology was detected using scanning electron microscopy following treatment with DCPIB or si-LRRC8A combined with PTX treatment in A2780 cells (scale bar, 10 μm). The experiments were analyzed using Dunnett's t-test. DCPIB, 4-(2-butyl-6,7-dichloro-2-cyclopentyl-indan-1-on5-yl) oxobutyric acid; si-, small interfering; LRRC8A, leucine-rich repeat-containing 8a; PTX, paclitaxel; LDH, lactate dehydrogenase.

pyroptosis process is that the mechanisms of pyroptosis are different in cancer and immune cells with different stimuli. LPS plus nigericin triggered caspase-1/GSDMD-dependent pyroptosis in BMDM cells (16), while PTX activated caspase-3/GSDME-dependent pyroptosis. It has also been reported that different chemotherapeutic agents may induce different secondary pyroptosis even in the same cell line with GSDME expression (20,45). In addition, the cancer cells
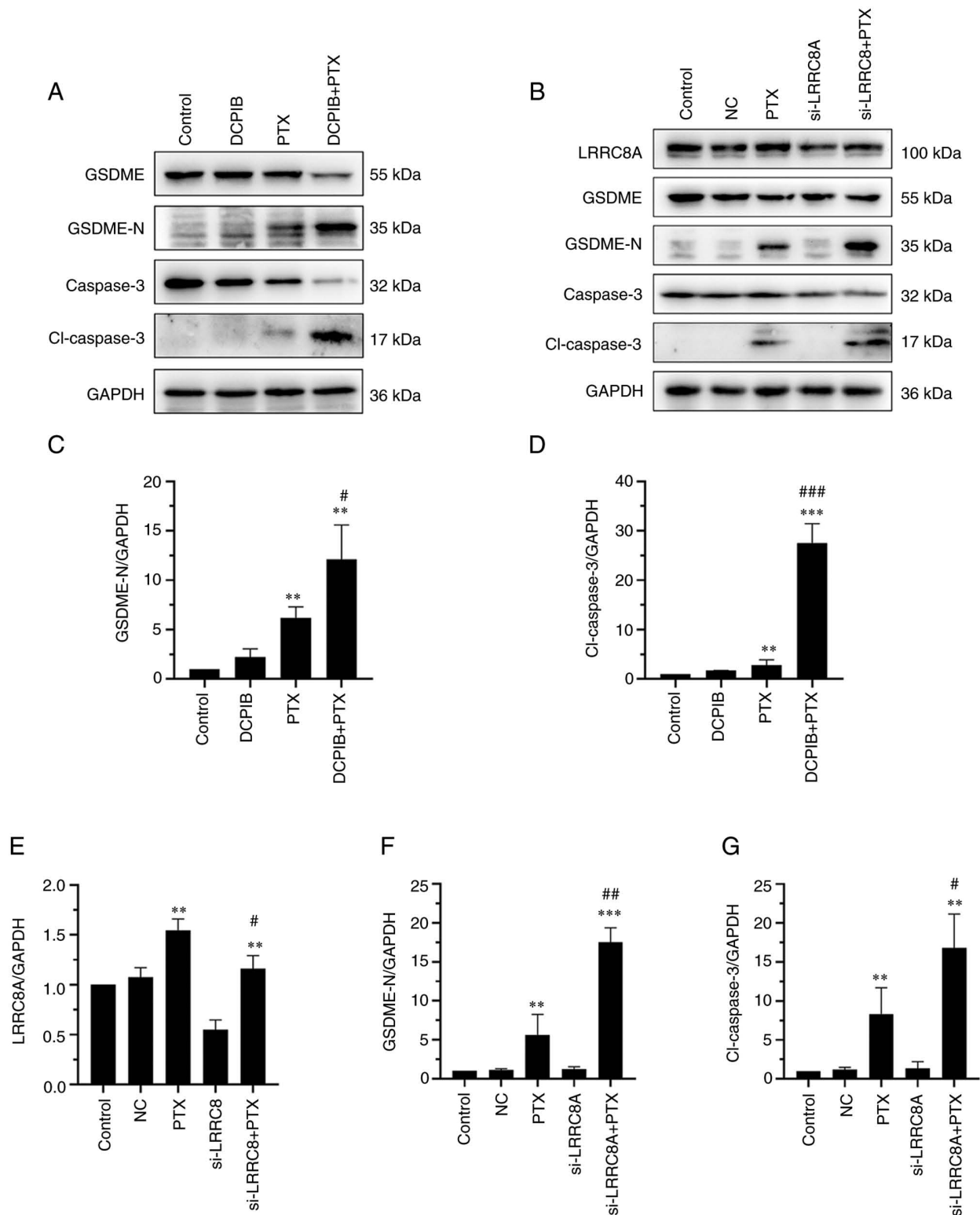
Figure 6. Effects of VRAC inhibitors and silencing of LRRC8A combined with PTX on pyroptosis-related proteins. (A) Representative western blotting and (C and D) analyzed data was used to detect the effect of PTX combined with DCPIB on the expression of GSDME-N and cl-caspase-3 proteins (n=3; **P<0.01 and ***P<0.001 vs. Control; #P<0.05 and ###P<0.001 vs. the PTX group). (B) Representative western blotting results and (E-G) analyzed data was used to detect the effects of PTX on the expression of LRRC8A, GSDME-N and cl-caspase-3 proteins by LRRC8A siRNA treatment (n=3; **P<0.01 and ***P<0.001 vs. Control; #P<0.05 and ##P<0.01 vs. the PTX group). The experiments were analyzed using Dunnett's t-test. VRAC, volume-regulatory anion channel; LRRC8A, leucine-rich repeat-containing 8a; PTX, paclitaxel; GSDME-N, cleaved-gasdermin E N-terminal fragment; DCPIB, 4-(2-butyl-6,7-dichloro-2-cyclopentyl-indan-1-on5-yl) oxobutyric acid; siRNA or si-, small interfering RNA.

exhibited more adaptive changes than normal cells. PTX induced an increase in the expression of LRRC8A which may be associated with its adaption in ovarian cancer cells, since ongoing experiments by the authors found that LRRC8A was overexpressed in PTX-resistant cell lines (data not shown). Therefore, whether individual characteristics of differential

chloride channel expression in ovarian cancer are associated with different degrees of PTX-induced pyroptosis will be investigated in the future.

In conclusion, caspase-3 was activated and specifically cleaved GSDME following PTX treatment to form a large number of membrane pores, and water molecules entered the cell causing cell swelling and inducing pyroptosis-like phenotypes. In addition, PTX and DCPIB increase the intracellular [Cl-]i by blocking the VRAC channel (LRRC8), which further promotes water entry and reduces water outflow, disrupting the osmotic balance and ultimately leading to persistent cell swelling (Fig. S2). PTX-induced pyroptosis was more effective when combined with the VRAC blocker or LRRC8A knockdown, the essential component of VRACs in A2780 ovarian cancer cells. These findings revealed a potential mechanism of PTX, and identified a combination of PTX and VRAC blockers that can synergistically treat ovarian cancer. However, in order to optimize their use in cancer treatment, whether the combination of PTX and VRAC blockers can harm non-tumorous cells needs to be determined.

Acknowledgements

Availability of data and materials

The datasets used and/or analyzed during the present study are available from the corresponding author on reasonable request.

Authors' contributions

XY and CL contributed equally to this work. XY and CL designed the study, performed the experiments and interpreted the data. XY wrote the manuscript. SL and XLiao performed statistical analyses.KW and XLi revised the manuscript. LZ, GL and HY contributed to the conception of the work, supervised the study design, and corrected the manuscript. XY and CL confirm the authenticity of all the raw data. All authors have read and agreed to the published version of the manuscript.

Ethics approval and consent to participate

Not applicable.

Patient consent for publication

Not applicable.

Competing interests

The authors declare that they have no competing interests.

References

1. Shao F: Gasdermins: Making pores for pyroptosis. Nat Rev Immunol 21: 620-621, 2021.
2. Shi J, Zhao Y, Wang K, Shi X Wang Y, Huang H, Zhuang Y, Cai T, Wang F and Shao F: Cleavage of GSDMD by inflammatory caspases determines pyroptotic cell death. Nature 526: 660-665, 2015.
3. Kayagaki N, Stowe IB, Lee BL, O'Rourke K, Anderson K, Warming S, Cuellar T, Haley B, Roose-Girma M, Phung QT, et al: Caspase-11 cleaves gasdermin D for non-canonical inflammasome signalling. Nature 526: 666-671, 2015.
4. Rogers C, Fernandes-Alnemri T, Mayes L, Alnemri D, Cingolani G and Alnemri ES: Cleavage of DFNA5 by caspase-3 during apoptosis mediates progression to secondary necrotic/pyroptotic cell death. Nat Commun 8: 14128, 2017.
5. Kovacs SB and Miao EA: Gasdermins: Effectors of Pyroptosis. Trends Cell Biol 27: 673-684, 2017.
6. Kepp O, Galluzzi L, Zitvogel L and Kroemer G: Pyroptosis-a cell death modality of its kind? Eur J Immunol 40: 627-630, 2010.
7. Okada Y, Okada T, Sato-Numata K, Islam MR, Ando-Akatsuka Y, Numata T, Kubo M, Shimizu T, Kurbannazarova RS, Marunaka Y and Sabirov RZ: Cell volume-activated and volume-correlated anion channels in mammalian cells: Their biophysical, molecular, and pharmacological properties. Pharmacol Rev 71: 49-88, 2019.
8. Okada Y, Sato K and Numata T: Pathophysiology and puzzles of the volume-sensitive outwardly rectifying anion channel. J Physiol 587: 2141-2149, 2009.
9. Zhang H, Li H, Liu E, Guang Y, Yang L, Mao J, Zhu L, Chen L and Wang L: The AQP-3 water channel and the ClC-3 chloride channel coordinate the hypotonicity-induced swelling volume in nasopharyngeal carcinoma cells. Int J Biochem Cell Biol 57: 96-107, 2014.
10. Zhou C, Tang X, Xu J, Wang J, Yang Y, Chen Y, Chen L, Wang L, Zhu L and Yang H: Opening of the CLC-3 chloride channel induced by dihydroartemisinin contributed to early apoptotic events in human poorly differentiated nasopharyngeal carcinoma cells. J Cell Biochem 119: 9560-9572, 2018.
11. Ye D, Luo H, Lai Z, Zou L, Zhu L, Mao J, Jacob T, Ye W, Wang L and Chen L: ClC-3 chloride channel proteins regulate the cell cycle by up-regulating cyclin D1-CDK4/6 through suppressing p21/p27 expression in nasopharyngeal carcinoma cells. Sci Rep 6: 30276, 2016.
12. Jentsch TJ: VRACs and other ion channels and transporters in the regulation of cell volume and beyond. Nat Rev Mol Cell Biol 17: 293-307, 2016.
13. Yang L, Ye D, Ye W, Jiao C, Zhu L, Mao J, Jacob TJC, Wang L and Chen L: ClC-3 is a main component of background chloride channels activated under isotonic conditions by autocrine ATP in nasopharyngeal carcinoma cells. J Cell Physiol 226: 2516-2526, 2011.
14. Cao G, Zuo W, Fan A, Zhang H, Yang L, Zhu L, Ye W, Wang L and Chen L: Volume-sensitive chloride channels are involved in maintenance of basal cell volume in human acute lymphoblastic leukemia cells. J Membr Biol 240: 111-119, 2011.
15. Yang L, Zhu L, Xu Y, Zhang H, Ye W, Mao J, Chen L and Wang L: Uncoupling of K+ and Cl- transport across the cell membrane in the process of regulatory volume decrease. Biochem Pharmacol 84: 292-302, 2012.
16. Ye X, Liu X, Wei W, Yu H, Jin X, Yu J, Li C, Xu B, Guo X and Mao J: Volume-activated chloride channels contribute to lipopolysaccharide plus nigericin-induced pyroptosis in bone marrow-derived macrophages. Biochem Pharmacol 193: 114791, 2021.
17. Yang F, Bettadapura SN, Smeltzer MS, Zhu H and Wang S: Pyroptosis and pyroptosis-inducing cancer drugs. Acta Pharmacol Sin 43: 2462-2473, 2022.
18. Gregory RE and DeLisa AF: Paclitaxel: A new antineoplastic agent for refractory ovarian cancer. Clin Pharm 12: 401-415, 1993.
19. Wang X, Li H, Li W, Xie J, Wang F, Peng X, Song Y and Tan G: The role of Caspase-1/GSDMD-mediated pyroptosis in Taxol-induced cell death and a Taxol-resistant phenotype in nasopharyngeal carcinoma regulated by autophagy. Cell Biol Toxicol 36: 437-457, 2020.
20. Zhang CC, Li CG, Wang YF, Xu LH, He XH, Zeng QZ, Zeng CY, Mai FY, Hu B and Ouyang DY: Chemotherapeutic paclitaxel and cisplatin differentially induce pyroptosis in A549 lung cancer cells via caspase-3/GSDME activation. Apoptosis 24: 312-325, 2019.

21. Zeng QZ, Yang F, Li CG, Xu LH, He XH, Mai FY, Zeng CY, Zhang CC, Zha QB and Ouyang DY: Paclitaxel enhances the innate immunity by promoting NLRP3 inflammasome activation in macrophages. Front Immunol 10: 72, 2019.

22. Feng J, Peng Z, Gao L, Yang X, Sun Z, Hou X, Li E, Zhu L and Yang H: ClC-3 promotes paclitaxel resistance via modulating tubulins polymerization in ovarian cancer cells. Biomed Pharmacother 138: 111407, 2021.

23. Mao J, Yuan J, Wang L, Zhang H, Jin X, Zhu J, Li H, Xu B and Chen L: Tamoxifen inhibits migration of estrogen receptor-negative hepatocellular carcinoma cells by blocking the swelling-activated chloride current. J Cell Physiol 228: 991-1001, 2013.

24. Xu R, Wang X and Shi C: Volume-regulated anion channel as a novel cancer therapeutic target. Int J Biol Macromol 159: 570-576, 2020.

25. Livak KJ and Schmittgen TD: Analysis of relative gene expression data using real-time quantitative PCR and the 2(-Delta Delta C(T)) method. Methods 25: 402-408, 2001.

26. Wu D, Wei C, Li Y, Yang X and Zhou S: Pyroptosis, a new breakthrough in cancer treatment. Front Oncol 11: 698811, 2021.

27. Broz P, Pelegrin P and Shao F: The gasdermins, a protein family executing cell death and inflammation. Nat Rev Immunol 20: 143-157, 2020.

28. De Schutter E, Croes L, Ibrahim J, Pauwels P, de Beeck KO, Vandenabeele P and Camp GV: GSDME and its role in cancer: From behind the scenes to the front of the stage. Int J Cancer 148: 2872-2883, 2021.

29. Chen LX, Zhu LY, Jacob TJ and Wang LW: Roles of volume-activated Cl- currents and regulatory volume decrease in the cell cycle and proliferation in nasopharyngeal carcinoma cells. Cell Prolif 40: 253-267, 2007.

30. Voss FK, Ullrich F, Munch J, Lazarow K, Lutter D, Mah N, Andrade-Navarro MA, von Kries JP, Stauber T and Jentsch TJ: Identification of LRRC8 heteromers as an essential component of the volume-regulated anion channel VRAC. Science 344: 634-638, 2014.

31. Menzin AW, King SA, Aikins JK, Mikuta JJ and Rubin SC: Taxol (paclitaxel) was approved by FDA for the treatment of patients with recurrent ovarian cancer. Gynecol Oncol 54: 103, 1994.

32. Kelly WK, Curley T, Slovin S, Heller G, McCaffrey J, Bajorin D, Ciolino A, Regan K, Schwartz M, Kantoff P, et al: Paclitaxel, estramustine phosphate, and carboplatin in patients with advanced prostate cancer. J Clin Oncol 19: 44-53, 2001.

33. Cortazar P, Justice R, Johnson J, Sridhara R, Keegan P and Pazdur R: US food and drug administration approval overview in metastatic breast cancer. J Clin Oncol 30: 1705-1711, 2012.

34. Ranson M and Thatcher N: Paclitaxel: A hope for advanced non-small cell lung cancer? Expert Opin Investig Drugs 8: 837-848, 1999.

35. Zhao S, Tang Y, Wang R and Najafi M: Mechanisms of cancer cell death induction by paclitaxel: An updated review. Apoptosis 27: 647-667, 2022.

36. Shi J, Gao W and Shao F: Pyroptosis: Gasdermin-mediated programmed necrotic cell death. Trends Biochem Sci 42: 245-254, 2017.

37. Wang Y, Gao W, Shi X, Ding J, Liu W, He H, Wang K and Shao F: Chemotherapy drugs induce pyroptosis through caspase-3 cleavage of a gasdermin. Nature 547: 99-103, 2017.

38. Zhang X, Zhang P, An L, Sun N, Peng L, Tang W, Ma D and Chen J: Miltirone induces cell death in hepatocellular carcinoma cell through GSDME-dependent pyroptosis. Acta Pharm Sin B 10: 1397-1413, 2020.

39. Shen X, Wang H, Weng C, Jiang H and Chen J: Caspase 3/GSDME-dependent pyroptosis contributes to chemotherapy drug-induced nephrotoxicity. Cell Death Dis 12: 186, 2021.

40. Kittl M, Winklmayr M, Preishuber-Pflugl J, Strobl V, Gaisberger M, Ritter M and Jakab M: Low pH attenuates apoptosis by suppressing the volume-sensitive outwardly rectifying (VSOR) chloride current in chondrocytes. Front Cell Dev Biol 9: 804105, 2021.

41. Tang T, Lang X, Xu C, Wang X, Gong T, Yang Y, Cui J, Bai L, Wang J, Jiang W and Zhou R: CLICs-dependent chloride efflux is an essential and proximal upstream event for NLRP3 inflammasome activation. Nat Commun 8: 202, 2017.

42. Green JP, Yu S, Martin-Sanchez F, Pelegrin P, Lopez-Castejon G, Lawrence CB and Brough D: Chloride regulates dynamic NLRP3-dependent ASC oligomerization and inflammasome priming. Proc Natl Acad Sci USA 115: E9371-E9380, 2018.

43. Decher N, Lang HJ, Nilius B, Bruggemann A, Busch AE and Steinmeyer K: DCPIB is a novel selective blocker of I(Cl,swell) and prevents swelling-induced shortening of guinea-pig atrial action potential duration. Br J Pharmacol 134: 1467-1479, 2001.

44. Pedersen SF, Okada Y and Nilius B: Biophysics and physiology of the volume-regulated anion channel (VRAC)/volume-sensitive outwardly rectifying anion channel (VSOR). Pflugers Arch 468: 371-383, 2016.

45. Zeng CY, Li CG, Shu JX, Xu LH, Ouyang DY, Mai FY, Zeng QZ, Zhang CC, Li RM and He XH: ATP induces caspase-3/gasdermin E-mediated pyroptosis in NLRP3 pathway-blocked murine macrophages. Apoptosis 24: 703-717, 2019.